Electronic and nuclear magnetic anisotropy of cobalt-doped ZnO single-crystalline microwires

Adrien Savoyant, O. Pilone, S. Bertaina, Fabian Delorme, Fabien Giovannelli

Electronic and Nuclear Magnetic Anisotropy of Cobalt-doped ZnO Single-crystalline Microwires

A. Savoyant,[1] O. Pilone,[1] S. Bertaina,[1] F. Delorme,[2] and F. Giovannelli[2]

[1] *Aix-Marseille Université, CNRS, IM2NP UMR 7334, 13397 Marseille Cedex 20, France*
[2] *Université de Tours, CNRS, INSA CVL, GREMAN UMR 7347, IUT de Blois, 15 rue de la chocolaterie, CS 2903, 41029 Blois Cedex, France.*

Using electron paramagnetic resonance (EPR), we investigate the electronic and nuclear magnetic properties of ZnO:Co single crystals, grown by the optical furnace method. The high crystal quality of the studied samples allows for the determination of the full hyperfine and g tensors. We explain how the local magnetic anisotropy of the Co^{2+} impurities is used as a very fine probe for the local symmetry and crystal quality of the host. The temperature- and power-study of EPR intensities recorded in three static- and microwave-field configurations give a qualitative insight into the dynamics of spin-lattice and spin-spin relaxations. In addition, in the context of nanostructures, we explain how a detailed analysis of the intensities anisotropy can reveal the proportion of ordered and disordered phases.

PACS numbers: 61.72.uj, 75.30.Gw, 75.50.Pp, 76.30.Fc

I. INTRODUCTION

ZnO micro- and nanocrystals, doped or not with magnetic impurities, are very interesting materials for a wide range of applications[1–5], particularly because of their inverse and direct piezoelectric (PZ) properties combined with their semiconducting n-type character[6–10]. For example, if the contact between a ZnO micro-crystal and a metal results in a Schottky barrier, a micro-scaled mechanical-to-electrical convertor is realized. These PZ properties arise on the one hand from the ionic and binary character of ZnO and, on the other hand, from the absence of inversion symmetry at each site of the ZnO wurtzite structure. Different crystal-grain orientations within a given sample results in a destructive PZ effect, so that this latter is positively correlated with the crystal quality of the considered sample. The obtention of very high crystal quality ZnO micro- and nano-structures is thus a key point to maximize the direct and inverse PZ effects to be used in concrete applications.

Besides, inserting magnetic ions in such a PZ semiconductor could result in interesting magneto-electrical, magneto-optical or magneto-mechanical couplings[11–17]. Apart from these hoped-for magnetic properties, cobalt-doping of ZnO nanostructures is also realized for many other reasons: to reduce some intrinsic defects[18], to enhance the PZ response and dielectric constant[8,9], to improve crystal quality[19], etc., these different effects being certainly linked together. Aside of these cobalt-induced properties, this doping is also performed for probing crystallinity of single crystals[20] or orientation's coherence of a set of nanorods[21], subjects on which we will focus thereafter. In particular, the use of Electron Paramagnetic Resonance (EPR) techniques allows for detecting very low impurities contamination or weak crystal-grain disorientation, provided that the resonant centers are sufficiently diluted and display a notable magnetic anisotropy. This is the case of ZnO:Co diluted magnetic semiconductor in which, at low temperature, the localized electronic spin of Co^{2+} shows a preferred orientation within the hexagonal plane of the wurtzite structure. The effective g-factor in a direction perpendicular to the $c-$axis is about twice that in the parallel direction. As a consequence, each local environment around a Co^{2+} ion gives EPR lines at a specific position, depending on its environment's orientation. Then, the total EPR spectrum contains information about the orientation's distribution, which can be extracted from suitable simulation. However, when dealing with very few numbers of paramagnetic impurities (as often in a nanostructure context), high-power microwave is required in order to detect something. This often leads to a saturated regime beyond the current-simulation possibilities. Thus, experimental reference spectra of single crystals for any microwave power are desirable data for understanding the saturated regime of nanostructures.

In this paper, we present the EPR results obtained on ZnO:Co single crystalline microwire (MW), grown by the optical furnace method. In this material, the nuclear hyperfine interaction of the $^{59}Co^{2+}$ ions displays a quite unusual large anisotropy ($A_{\parallel}/A_{\perp} = 5.4$). Due to its low value in the perpendicular direction ($A_{\perp} = 2.98 \times 10^{-4}$ cm$^{-1} \equiv 0.3$ mT), the full hyperfine tensor can only be resolved in very high crystal-quality samples, for which the EPR line width is significantly lower than 0.3 mT. We show that such a crystal quality can be reached in the studied material, which allows for the electronic and nuclear magnetic anisotropy characterization, through the

determination of the full g-factor and hyperfine tensors. Three different static- and microwave-field configurations are used, for which the temperature and microwave-power dependence are studied. The fits of the temperature-dependent intensities confirm the correctness of the spin 3/2 model for each configuration, while the power-dependent intensities curves reveal the different dynamics of each. Qualitative analysis of these data shows that the spin-lattice relaxation time $\mathcal{T}_1$ has axial anisotropy, while the spin-spin one $\mathcal{T}_2$ is almost isotropic. Then, in the wider context of nanostructures, we explain how the power-study of the intensity ratio $I_{\parallel}/I_{\perp}$ allows for the separation between signals arising from ordered and disordered phases when working in an EPR saturated regime.

II. EXPERIMENTAL

The wurtzite-crystallized ZnO:Co MW under study has been grown by the optical furnace method, described in previous papers[20,22]. The SEM image in Fig. 1 shows a typical MW, with its hexagonal cross section. In all cases, the c-axis of the wurtzite structure is parallel to the long dimension of the MW, which is also taken to be the z-axis of the laboratory frame (see Fig. 1). In order to obtain the smallest EPR line width necessary to resolve the perpendicular hyperfine coupling ($A_{\perp} \equiv 0.3$ mT), the least Co-doped MW was chosen, among the completely transparent ones (green coloration increases with Co-doping[20]). Thus, dipolar broadening is at its minimum and only excited-level lifetime and structural disorder, respectively, contribute to homogeneous and inhomogeneous EPR line broadening. For the intensity measurements in the three configurations, another MW slightly more doped has been used: in this one, all intensities are increased but also the line width so that the perpendicular hyperfine coupling $A_{\perp}$ is not resolved.

The X-band ($\nu = 9.621$ GHz) EPR spectra were recorded using a Bruker EMX spectrometer equipped with a standard TE_{102} cavity. The low temperature (5 K) equilibrium was obtained by using a continuous helium-flow cryostat stabilized with an Intelligent Temperature Controller (Oxford, ITC 503). Regarding the orientation of the static ($\mathbf{B}$) and of the microwave ($\mathbf{B}_1$) fields with respect to the c-axis of the wurtzite MW, three configurations are possible, depicted in Fig. 1 and denoted by $C_{\parallel}$, $C_{\perp}$ and $C'_{\perp}$. Each of them gives a particular EPR intensity, with its own power- and temperature-dependence.
Sensitivity improvement was achieved by the use of a lock-in amplifier modulating the static $\mathbf{B}$-field at a 100 kHz frequency. The amplitude of this modulation was set to always avoid over-modulation phenomena (while keeping sufficiently intense signal) down to 0.05 mT. Regarding the saturation recovery measurements, the incident microwave power P was controlled by an attenuation $\mathcal{A} = 10\log(P_0/P)$, with $P_0 = 200$ mW.
ZnO:Co MW images were performed in a FEI Quanta 200 scanning electron microscope (SEM).

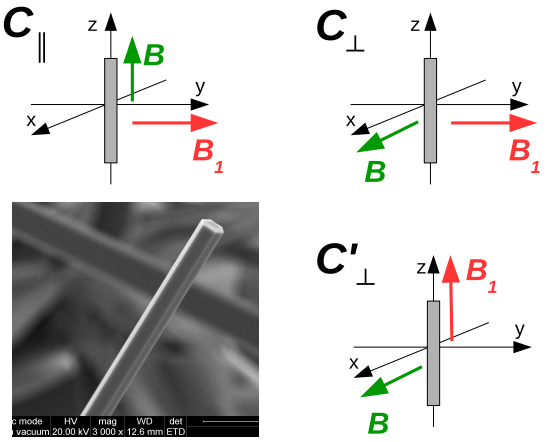

Figure 1: (color online) Top and bottom-right: Schematic of the three field-configurations, $C_{\parallel}$, $C_{\perp}$ and $C'_{\perp}$, with respect to the $c-$axis ($\parallel z$) of the wurtzite MW. Bottom-left: SEM image of individual ZnO:Co microcrystal showing the hexagonal section.

III. RESULTS

A. Experimental and simulated spectra

The experimental spectra of the ZnO:Co MWs recorded at $T = 5$ K in the $C_{\parallel}$ and $C_{\perp}$ field configurations are shown in Fig. 2 for high and low microwave power. The $C'_{\perp}$ configuration spectrum is not shown because of the too low signal/noise ratio (see Sec. III C). No other signal than the Co-related one is detected, indicating the absence of contamination with paramagnetic impurities. In particular, none of the intrinsic defects observed in ZnO nanostructures are detected. The anisotropy of the $S = 3/2$ electronic spin of the Co^{2+} ion is clearly seen by the different spectra position for the two orientations, while that of the hyperfine coupling is represented by the different spacing between two adjacent lines of the octet spectrum. Such spectra can be simulated by the following spin Hamiltonian, acting in the 32-dimensional space produced by the electronic and nuclear spins, $S = 3/2$ and $I = 7/2$ respectively:

$$H = DS_z^2 + \mu_B \overrightarrow{S}.\tilde{g}.\overrightarrow{B} + \overrightarrow{S}.\tilde{A}.\overrightarrow{I} \qquad (1)$$

This Hamiltonian includes, respectively, the

uniaxial anisotropy ($D > 0$, easy plane), the Zeeman interaction ($\tilde{g}$) and the hyperfine coupling ($\tilde{A}$). The principal components of the $\tilde{g}$ and $\tilde{A}$ tensors can be directly read on these spectra, without any simulation, and independently of the microwave power. These are in accordance with the usual ZnO:Co values, $g_{\parallel} = g^{\parallel}_{eff} = 2.256$ and $g_{\perp} = g^{\perp}_{eff}/2 = 2.283$, $A_{\parallel} = 16.07 \times 10^{-4}$ cm^{-1} and $A_{\perp} = 2.98 \times 10^{-4}$ cm^{-1}. We remark that the measurement of the $A_{\perp}$ value necessitates a very low line width (< 0.3 mT), only reachable in very high quality single crystals. Only three previous works have reported such a measurement on ZnO:Co, Estle & De Wit (bulk material, 1967)[23], Hausmann (bulk material, 1969)[24] and Jedrecy *et al.* (thin film, 2004)[25]. Here, the crystal quality is such that the apparent EPR line width is as low as 0.08 mT, allowing for a precise determination of $A_{\perp}$. This value can be used for simulation of low-resolved spectra. The determination of the axial anisotropy parameter D can not be directly performed with such X-band EPR spectra, but a relation linking it to the difference $\Delta g = g_{\perp} - g_{\parallel} = 0.027$ has been derived in a previous work[21], which gives an identical result here ($D = 2.57$ cm^{-1}).

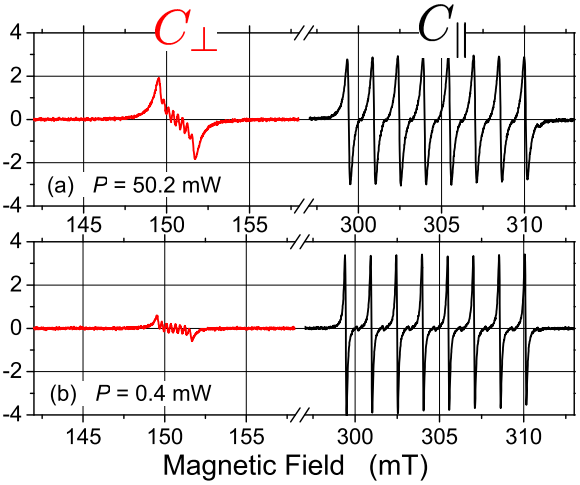

Figure 2: (color online) EPR spectra of ZnO:Co MW in $C_{\perp}$ (left, red) and $C_{\parallel}$ (black, right) configurations, recorded in saturating (a) and off-saturating (b) conditions, at $T = 5$ K. All intensities are normalized.

While these spin Hamiltonian parameters are intrinsically power-independent, we observe that the EPR line width and intensities vary with the incident microwave power (Fig. 2). This is because these are characteristics of the EPR resonance phenomena described by the time-dependent Hamiltonian $H_1(t) = \mu_B S.\tilde{g}.B_1(t)$, with $B_1 \propto \sqrt{P}$, and not of the material itself. Line width reaches its minimum as the incident power goes to zero, when the resonance is not saturated. The intensities (double integration of spectra) obtained in $C_{\parallel}$ and $C_{\perp}$ configurations appear to depend on the incident microwave power, as well as their ratio $I_{\parallel}/I_{\perp}$. Within the experimental power range, this ratio varies between 1 and 2; this cannot be accounted for by spectra simulation. Indeed, spectra obtained by simulation softwares as Easyspin[26] do not include power dependence, which relies on complex relaxation phenomena, but do describe a non-saturating limit, when P tends to zero and intensity is proportional to $\sqrt{P}$. By trying to simulate the two-orientations spectra of figure 2, only that with the lowest microwave power ($P = 0.4$ mW) gives a satisfactory result (Fig. 3) indicating a non-saturating regime. No parameter adjustment allows for a reasonable fit of the high power ($P = 50.2$ mW) measurement, which is then supposed to be saturated, out of current-simulation possibilities.

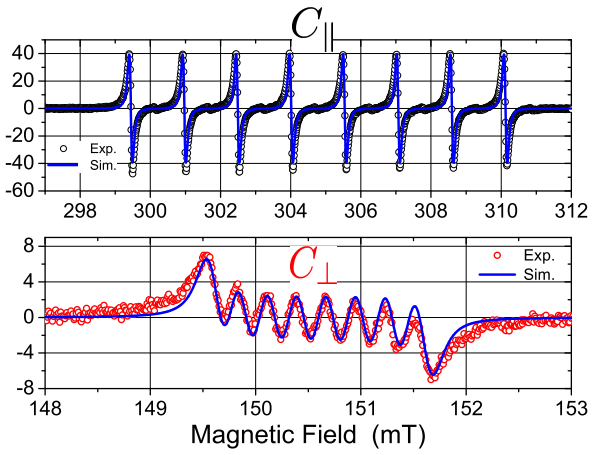

Figure 3: (color online) Experimental EPR spectra of the ZnO:Co MW in $C_{\parallel}$ (up, black circles) and $C_{\perp}$ (down, red circles) configurations, recorded at $T = 5$ K and $P = 0.4$ mW (same data as Fig 2-b). Blue lines show simulated spectra from Eq. 1 with parameters discussed in the text.

The best obtained simulation with Easyspin[26] shown in figure 3 includes a slight g-strain within the hexagonal cross section, that is a normalized narrow gaussian distribution of $g_{\perp}$ values of $\delta g_{\perp} = 0.002$ width. This g-strain is likely to arise from minute stress within the hexagonal MW section. We remark that the line shape is Lorentzian, indicating a predominance of homogeneous broadening. The global agreement between simulated and off-saturation experimental spectra in both configurations $C_{\parallel}$ and $C_{\perp}$ is satisfactory, so that we conclude that the $S = 3/2$ and $I = 7/2$ model coupled to the Hamiltonian (1) well describe substitutional Co^{2+} ions in ZnO.

B. Temperature dependence

In order to test the validity of the model in the three configurations $C_{\parallel}$, $C_{\perp}$, and $C'_{\perp}$, we examine the temperature dependence of their intensity obtained by the double-integration method. These measurements have been performed on another MW, a bit more cobalt-doped in order to increase the $C'_{\perp}$ EPR intensity, but with the consequence that the line width is increased so that the perpendicular hyperfine coupling is no longer resolved. However, this increase in the line width does not affect at all the intensities, which might be fitted by EPR intensity formulae as well. In off-saturating conditions, the EPR intensities in the three configurations are described by formula (2), (3) and (4). These take into account the transition probability and the Boltzmann population difference between the two resonating levels, but also the important frequency-to-field conversion factor[27,28] and the $\mathcal{T}_2^{\parallel}$ and $\mathcal{T}_2^{\perp}$ transverse relaxation times[30]. These latter can be passed in the K constant when fitting only one line, just as in Ref. 21, but not in the present case.

$$I_{\parallel}(T) = K\frac{g_{\perp}^2\mathcal{T}_2^{\perp}\sqrt{P}}{g_{\parallel}T(1+e^{-2D/kT})} \quad (2)$$

$$I_{\perp}(T) = K\frac{g_{\perp}\mathcal{T}_2^{\perp}\sqrt{P}}{2T(1+e^{-2D/kT})} \quad (3)$$

$$I'_{\perp}(T) = K\frac{g_{\parallel}^2\mathcal{T}_2^{\parallel}\sqrt{P}}{g_{\perp}8T(1+e^{-2D/kT})} \quad (4)$$

The K-factor takes account for all other experimental parameters (static-field modulation, etc.) identical in the three configurations. Although the same in the three configurations, the $\sqrt{P}$ dependence is explicitly written for completeness of the involved physical parameters. In order to reduce the number of parameters, we have fitted the experimental intensities by taking $\mathcal{T}_2^{\perp} = \mathcal{T}_2^{\parallel}$, so that only the common factor K has been adjusted to obtain the fit of figure 5. Considering the uncertainty on the intensity measurement (from about 5% at low temperature to 10% at high temperature), the fitting agreement can be considered as fully satisfactory. Taking into account different transverse relaxation times ($\mathcal{T}_2^{\parallel} \neq \mathcal{T}_2^{\perp}$) results in a very poor improvement of the fits, so that these two relaxation times may reasonably assumed to be almost identical.

As the temperature tends to zero, the theoretical ratio $I_{\parallel}/I_{\perp}$ (in non-saturating condition, $P = 0.4$ mW) tends to $2g_{\perp}/g_{\parallel}$, that is 2.05, to be compared with the experimental ratio of 1.94 at $T = 5$ K. The temperature dependence of this ratio is slight and not of great importance because the EPR intensity in the three configurations rapidly goes to zero (for relaxation reasons), as the temperature exceed 15 K. On the contrary, this $I_{\parallel}/I_{\perp}$ ratio highly depends on incident microwave power P, as discussed now.

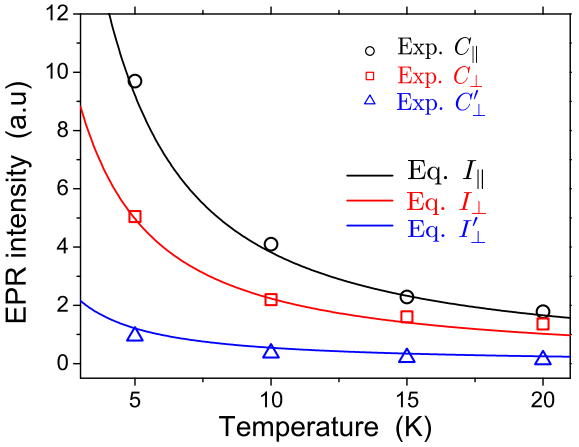

Figure 4: (color online) Open circles, squares and triangles: experimental EPR spectra intensities in $C_{\parallel}$, $C_{\perp}$ and $C'_{\perp}$ field configurations, recorded in non-saturating condition ($P = 0.4$ mW). Solid lines: corresponding calculated intensities from Eq. (2), (3) and (4).

C. Power dependence

Aside of the precise determination of the spin Hamiltonian parameters from EPR spectra simulations and the temperature dependence study, it is interesting to study the spin dynamics in the three configurations. Such information can be partially extracted from the study of the EPR intensity-saturation curves (Fig. 5). Off-saturation regime is characterized by an intensity proportional to $\sqrt{P}$ (see Eqs. (2), (3), (4)), thus appearing as straight lines at low power in figure 5. Saturation occurs when the rate of absorption become greater than the rate of relaxation, so that the Co^{2+} ions can no longer absorb all the incident photons. Indeed, for the absorption phenomenon to reach a stationary state, the excited state lifetime must be much smaller than the mean time between two photon incidences, this latter depending on microwave power. In other words, the faster a set of microwave-excited Co^{2+} ions go back to their ground state by evacuating quantized energy toward the lattice, the more it can absorb microwave power.

Qualitatively, the power saturation phenomenon arises naturally from the classical Bloch equations. In the simple case of isotropic magnetic moment and without any inhomogeneous broadenning, the

following factor can multiply the intensities (2), (3) and (4) in order to give account for the saturated regime[29]:

$$(1 + C.\mathcal{T}_1.\mathcal{T}_2.P)^{-1} \quad (5)$$

where C is a constant assumed to be identical in the three configurations, $\mathcal{T}_2$ is the isotropic transverse (along $\mathbf{B}_1$ field) relaxation time discussed before, and $\mathcal{T}_1$ the longitudinal (along $\mathbf{B}$ field), or spin-lattice, relaxation time. $\mathcal{T}_1$ is equal to its parallel ($\mathcal{T}_1^{\parallel}$) or perpendicular ($\mathcal{T}_1^{\perp}$) value, according to the $\mathbf{B}$-field orientation in the considered configuration (see Fig. 1). Then, qualitatively, the EPR phenomenon will enter a saturated regime even more rapidly as the $\mathcal{T}_1\mathcal{T}_2$ product gets larger, which will be visible in the saturation curves by departure from the straight dashed-line.

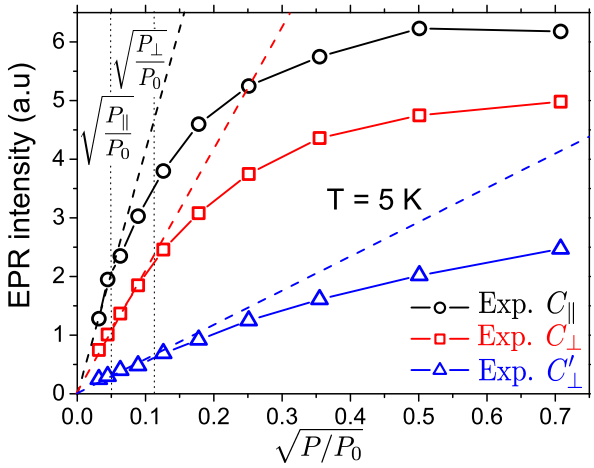

Figure 5: (color online) Saturation curves of EPR intensities recorded at $T = 5$ K and 0.5 G modulation for the three magnetic-field configurations. Dashed lines illustrate the off-saturating regime while dotted lines indicate saturation occurences.

Thus, recalling that $\mathcal{T}_2^{\parallel} = \mathcal{T}_2^{\perp}$, it is expected that $C_\perp$ and $C'_\perp$ configurations will saturate at the same power (because both have the same $\mathbf{B}$-field orientation) which is indeed observed in figure 5. On the other hand, $C_\parallel$ and $C_\perp$ configurations have different $\mathbf{B}$-field orientation, so that each of them is characterized by a different spin-lattice relaxation time, respectively $\mathcal{T}_1^{\parallel}$ and $\mathcal{T}_1^{\perp}$. As saturation occurs at lower power in the $C_\parallel$ configuration (see Fig. 5: $P_\parallel < P_\perp$), we deduce that $\mathcal{T}_1^{\parallel} > \mathcal{T}_1^{\perp}$. We can then conclude that there is some anisotropy in the spin-lattice coupling, which is stronger in the hexagonal plane (shorter relaxation) than along the c-axis of the wurtzite structure (longer relaxation). It must be stressed out that the considered relaxation times are phenomenological parameters arising from the classical isotropic Bloch equations, so that they can in fact include some other parameters such as the component of the effective $\tilde{g}$-tensor. Access to the real relaxation times can be quantitatively reached by the combination of pulsed EPR methods and fitting of the saturation curves including inhomogeneous phenomena, thus giving greater insight into the spin dynamics.

Another interesting information to be extracted from the saturation curves in figure 5 is the maximum power to which the resonance, in both configuration $C_\parallel$ and $C_\perp$, is off-saturation and can then be properly simulated by Easyspin software. Beyond this power, no adjustment of any parameter can give a satisfactory fitting. It is to be noted that this power can slightly depend on various experimental conditions, such as cavity quality-factor, sample volume, filling factor, etc, and must then be regarded as an approximate value. Figure 5 shows that the first apparition of saturated regime occurs in the $C_\parallel$ configuration at a power defined by $\sqrt{P_\parallel/P_0} = 0.05$, that is $P_\parallel = 0.5$ mW.

D. Intensities anisotropy

We now turn to the study of the $I_\parallel/I_\perp$ ratio. As pointed out before, this ratio only slightly depends on temperature in the range 5-10 K, but notably does on the incident microwave power (see Fig. 6). Starting from a non-saturating regime in which $I_\parallel/I_\perp \simeq 2$ at low temperature (around 5 K), each intensity increases as the incident microwave power is augmented, as shown in Fig. 5. However, due to different spin-lattice relaxation times in $C_\parallel$ and $C_\perp$ configurations, the increase has a different rate and maximum value in each case, so that the intensity ratio changes with power.

The strongest interest for the knowledge of this $I_\parallel/I_\perp$ ratio power-dependence in single a microcrystal is that this latter is equivalent to an ideally orientated set of nanorods or nanowires. In this context of ZnO:Co nanostructures, the number of spins is weak so that high incident microwave power is often required in order to obtain a detectable signal, leading to a saturated regime. Thus, a simple EPR simulation is not relevant and, as shown in a previous work[18], the experimental $I_\parallel/I_\perp$ ratio is systematically lower than 1, that is out of the figure 6 curve. The simplest interpretation for this deviation is that some other signal positively contributes to the $I_\perp$ intensity, thus leading to a reduction of the considered ratio. Indeed, this contribution is likely to arise from a disordered phase of the ZnO:Co nano-objects

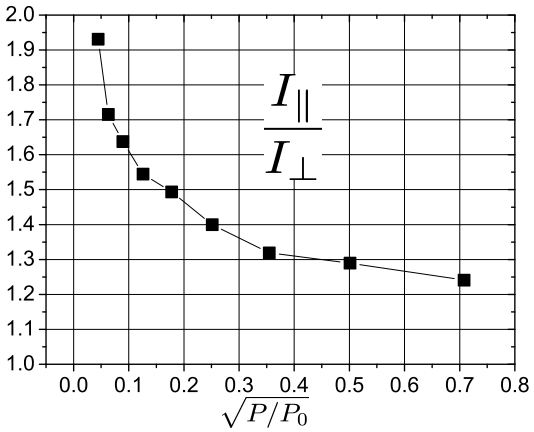

Figure 6: Evolution of the $I_{\parallel}/I_{\perp}$ intensities ratio as a function of the microwave power ($P_0 = 200$ mW), recorded at $T = 5$ K.

which, in the case of totally random orientations (powder), give the spectrum of Fig. 7-c, that is a single assymmetric line located at the same B-field as for the $C_{\perp}$ configuration ($\sim$ 150 mT). This hypothesis is strongly supported by the shape of the $I_{\perp}$ intensity observed in Ref. 18, which shows a pronounced asymmetry just as in the powder spectrum signal (Fig. 7).

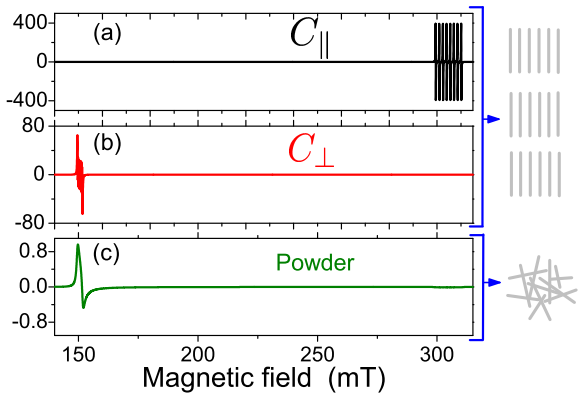

Figure 7: (color online) EPR spectra simulations of ideally orientated [(a) and (b)] and totally disordered (c) sets of ZnO:Co nanorods.

In this scenario, the ZnO:Co nanostructures EPR spectra would be the superposition of ordered- and disordered-phase signals. In a non-saturating resonance regime, the total signal can be simulated, which directly gives access to the proportion of ordered and disordered phases. However, as seen before, the maximum power for such a non-saturating case is very low (0.5 mW) so that, in many cases, the incident microwave power will be greater than that, which correspond to an abscissa greater than 0.05 in figure 6. Then, at such a given microwave power, the knowledge of the single-crystal $I_{\parallel}/I_{\perp}$ ratio would permit, if it exists, to determine the amount of non-ordered signal intensity at 150 mT. Appropriate simulation of this remaining intensity would thus allow for the approximate quantification of Co^{2+} ions in ordered and disordered phase. Refinement of this quantification could be reached by considering orientated powder, or other particular distribution of spin orientations, rather than a totally disordered phase. Finally, the only difficulty would be to correctly simulate the (oriented-) powder spectra for any microwave power, including the saturated regime.

IV. CONCLUSION

Electronic and nuclear magnetic properties of $^{59}Co^{2+}$ ions embedded in a tetrahedral local symmetry, as arising in ZnO:Co, show interesting and sizeable orientation dependence. In this paper, we have reported the use of these magnetic anisotropies for the crystal-quality characterization of low-doped ZnO:Co microcrystals. The use of three EPR configurations and the study of each resulting intensity temperature- and power-dependence have allowed for the validation of ($S = 3/2, I = 7/2$) model with easy-plane uniaxial electronic spin anisotropy. By the way, these studies have shown that the phenomenological spin-spin relaxation time must be isotropic, while the spin-lattice relaxation time appears to be anisotropic, with $\mathcal{T}_1^{\parallel} > \mathcal{T}_1^{\perp}$. Finally, in the context of orientated nanostructures as nanorods or nanowires, we have shown how the power dependence of the $I_{\parallel}/I_{\perp}$ ratio can reveal the proportion of ordered and disordered phases.

V. ACKNOWLEDGEMENT

This work was supported by the NATO project Science for Peace (SfP) 984735, Novel nanostructures. A. Savoyant acknowledges Prof. André Ghorayeb for fruitful discussions and corrections.

[1] H. Ohno, Science **281**, 951 (1998).
[2] Žutić I, Fabian J and das Sarma S 2004 *Rev. Mod. Phys.* **76** 323
[3] Gu Y, Kuskovsky I L, Yin M, O'Brian S and Neu-

mark G F 2004 *Appl. Phys. Lett.* **85** 3833
[4] Willander M, *et al* 2009 *Nanotechnology* **20** 332001
[5] U. Ozgur, D. Hofstetter and H. Morkoc, *Proc. IEEE* vol. **98**, no. 7 , pp. 1255-1268, 2010.
[6] Z. L. Wang and J. Song, *Science* **312**, 242 (2006).
[7] Y. Xi, J. Song, S. Xu, R. Yang, Z. Gao, C. Hu, and Z. L. Wang, *J. Mater. Chem.*, 2009, **19**, 9260-9264.
[8] H. Parangusan, D. Ponnamma, and M. Al Ali Al-Maadeed, *Sci. Rep.* **8**, 754 (2018).
[9] W. Zang, P. Li, Y. Fu, L. Xing, and X. Xue, *RSC Adv.*, 2015, **5**,84343.
[10] K. Momeni, G. M. Odegard, and R. S. Yassar, *Acta Materialia* **60** (2012), 5117-5124.
[11] Duan L B, Chu W G, Yu J, Wang Y C, Zhang L N, Liu G Y, Liang J K and Rao G H 2008 *J. Magn. Magn. Mater.* **320** 1573
[12] Lin C Y, Wang W H, Lee C-S, Sun K W and Suen Y W *App. Phys. Lett.* **94**, 151909 (2009)
[13] Gandhi V, Ganesan R, Syedahamed H H A and Thaiyan M, *J. Phys. Chem. C* **2014**, 118 (18), pp 9715-9725
[14] Kumar S, Song T K, Gautam S, Chae K H, Kim S S and Jang K W 2015 *Mat. Res. Bull* **66** 76
[15] Chanda A, Gupta S, Vasundhara M, Joshi S R, Mutta G R and Singh J, *RSC Adv.* 2017, **7**, 50527-50536
[16] S. M. Siagian *et al.* 2017 *J. Phys.: Conf. Ser.* **795** 012009.
[17] P. Sati *et al.* 2006 *phys. Rev. Lett.* **96** 017203.
[18] A. Savoyant, H. Alnoor, O. Pilone, O. Nur, and M. Willander, *Nanotechnology* **28**, 285705 (2017)
[19] C.-W Liu, S-J Chang, S. Brahma, C-H Hsiao, F. M. Chang, P. H. Wang, and K-Y Lo, *J. Appl. Phys.* **117**, 084315 (2015).
[20] A. Savoyant, F. Giovannelli, F. Delorme, and A. Stepanov, *Semicond. Sci. Technol.* **30** (2015) 075004.
[21] A. Savoyant, H. Alnoor, S. Bertaina, O. Nur, and M. Willander, *Nanotechnology* **28**, 035705 (2017)
[22] F. Giovannelli, G. Rajonson, J. Wolfman, and F. Delorme, *Mater. Lett.* **107**, 194 (2013).
[23] T. Estle, M. De Wit, Bull. Am. Phys. Soc. **6**, 445 (1961).
[24] A. Hausmann, *Phys. Status Solidi* **31** (1969) K131.
[25] N. Jedrecy, H. J. von Bardeleben, Y. Zheng, and J-L. Cantin, *Phys. Rev.* B **69**, 041308(R) (2004).
[26] S. Stoll and A. Schweiger, *J. Magn. Reson.* **178**, 42 (2006).
[27] J. R. Pilbrow, *J. Magn. Reson.* **58**, 186 (1984).
[28] R. Aasa and T. Vänngård, *J. Magn. Reson.* **19**, 308 (1975).
[29] J. A. Weil and J. R. Bolton, *Electron Paramagnetic Resonance*, Wiley-Interscience p. 314.
[30] $\mathcal{T}_2$ times characterizes the relaxation time along the microwave field B_1 direction, with *a priori* two possible values in an axial-anisotropy case, $\mathcal{T}_2^{\parallel}$ and $\mathcal{T}_2^{\perp}$.